

p53 genes (27, 28), underscoring their evolutionary relatedness.

8. We screened 48,000 wild-type (N2) genomes for a *cep-1* deletion using 4,5',8-trimethylpsoralen/ultraviolet light mutagenesis as described (29, 30). First-round polymerase chain reaction primers flanking *cep-1* were 5'-GGTGGACTGTTCGCTTGAATCAA-GACTGC-3' and 5'-GCTCTTGATGTGCCAACAA-GATCGGATTC-3'. Second-round primers were 5'-CAGGGGAGTTGGCGTTAGG-3' and 5'-AATTGGTA-CAGCGACTTCTCTTCA-3'. A single worm containing the *cep-1(w40)* deletion was identified. This deletion removes 1823 nucleotides of the gene, corresponding to nucleotides 28,754 to 31,967 on cosmid F52B5. The splice acceptor and donor sites remain intact in the *cep-1(w40)* allele, which is predicted to encode an in-frame but truncated protein missing amino acids 69 to 242. Further analysis showed that the deletion strain also carries an intact copy of *cep-1*. The *w40* allele segregates independently of the wild-type *cep-1* locus, indicating that the deleted copy had translocated to another region of the genome and a wild-type copy of *cep-1* remains at the normal locus.
9. A. Fire *et al.*, *Nature* **391**, 806 (1998).
10. W. B. Derry, J. H. Rothman, unpublished data.
11. A. Gartner, S. Milstein, S. Ahmed, J. Hodgkin, M. O. Hengartner, *Mol. Cell* **5**, 435 (2000).
12. T. L. Gumienny, E. Lambie, E. Hartweg, H. R. Horvitz, M. O. Hengartner, *Development* **126**, 1011 (1999).
13. D. G. Albertson, A. M. Rose, A. M. Villeneuve, in *C. elegans II*, D. L. Riddle, T. Blumenthal, B. J. Meyer, J. R. Priess, Eds. (Cold Spring Harbor Laboratory Press, Cold Spring Harbor, NY, 1997), pp. 47-78.
14. To determine the expression pattern of *cep-1*, we designed a reporter construct that includes 4.5 kb of sequence upstream of the start codon as well as the entire CEP-1 coding sequence, fused in-frame to GFP. The *cep-1* sequences were obtained by amplification from cosmid F52B5 and cloned into vector pPD 96.04. Reporter constructs were coinjected with the dominant *rol-6(su1006)* marker gene to create transgenic lines (31). This results in repetitive arrays that are generally silenced in the germ line; thus, the marker is likely to reveal the zygotic expression exclusively.
15. T. Jacks *et al.*, *Curr. Biol.* **4**, 1 (1994).
16. A. Rogel, M. Popliker, C. G. Webb, M. Oren, *Mol. Cell Biol.* **5**, 2851 (1985).
17. P. Schmid, A. Lorenz, H. Hameister, M. Montenarh, *Development* **113**, 857 (1991).
18. J. B. Wallingford, D. W. Seufert, V. C. Virta, P. D. Vize, *Curr. Biol.* **7**, 747 (1997).
19. T. G. Graeber *et al.*, *Mol. Cell Biol.* **14**, 6264 (1994).
20. R. Alarcón, C. Koumenis, R. K. Geyer, C. G. Maki, A. J. Giaccia, *Cancer Res.* **59**, 6046 (1999).
21. Genomic *cep-1* was amplified from cosmid F52B5 using primers tagged with a Kpn I site 5' of the ATG start codon and a Sac I site after the stop codon and cloned into vectors pPD 49.78 (*hsp16-2*) and pPD 49.83 (*hsp16-41*). Transgenic lines were established by standard methods (31). The primers were 5'-GCGGTACCATGAATTTGAATGAAGATTG-3' and 5'-CCGAGCTCTACTTTGGCAGTTTCATCG-3'. CEP-1 was overexpressed in transgenic worms by subjecting them to a 15- to 20-min heat shock at 34°C (32).
22. H. M. Ellis, H. R. Horvitz, *Cell* **44**, 817 (1986).
23. J. M. Abrams, K. White, L. I. Fessler, H. Steller, *Development* **117**, 29 (1993).
24. C. Kitahana, Y. Kuchino, *Cell Death Differ.* **6**, 508 (1999).
25. S. F. Altschul *et al.*, *Nucleic Acids Res.* **25**, 3389 (1997).
26. S. Henikoff, J. G. Henikoff, W. J. Alford, S. Pietrokovski, *Gene* **163**, 17 (1995).
27. B. Bienz, R. Zakut-Houri, D. Givol, M. Oren, *EMBO J.* **3**, 2179 (1984).
28. P. Lamb, L. Crawford, *Mol. Cell Biol.* **6**, 1379 (1986).
29. G. Jansen, E. Hazendonk, K. L. Thijssen, R. H. A. Plasterk, *Nature Genet.* **17**, 119 (1997).
30. K. Gengyo-Ando, S. Mitani, *Biochem. Biophys. Res. Commun.* **269**, 64 (2000).
31. C. C. Mello, J. M. Kramer, D. Stinchcomb, V. Ambros, *EMBO J.* **10**, 3959 (1991).

32. E. G. Stringham, D. K. Dixon, D. Jones, E. P. M. Candido, *Mol. Biol. Cell* **3**, 221 (1992).
33. A. Sali, T. L. Blundell, *J. Mol. Biol.* **234**, 779 (1993).
34. Y. Cho, S. Gorina, P. D. Jeffrey, N. P. Pavletich, *Science* **265**, 346 (1994).
35. J. Lin, J. Chen, B. Elenbaas, A. J. Levine, *Genes Dev.* **8**, 1235 (1994).
36. C. J. Thut, J. L. Chen, R. Klemm, R. Tjian, *Science* **267**, 100 (1995).
37. We thank M. Fukuyama for help with the deletion screen, C. Farmer and the Tri-Counties Blood Bank for use of their gamma source, R. Christoffersen for hypoxic chambers, S. Roberts for providing the three-dimensional model, R. Halberg for useful discussions,

A. Fire for vectors, and A. Coulson for cosmid. Some of the strains were provided by the *Caenorhabditis* Genetics Center, which is funded by the National Center for Research Resources of NIH. Supported by the Cancer Center of Santa Barbara and the Tri-Counties Blood Bank (W.B.D.) and grants from Santa Barbara Cottage Hospital, the University of California Cancer Research Coordinating Committee, and National Institute on Aging grant AG13736 (J.H.R.).

17 August 2001; accepted 3 September 2001
 Published online 13 September 2001;
 10.1126/science.1065486
 Include this information when citing this paper.

Integration Between the Epibranchial Placodes and the Hindbrain

Jo Begbie and Anthony Graham*

Developmental integration results from coordination among components of different embryonic fields to realize the later anatomical and functional relationships. We demonstrate that in the chick head, integration between the epibranchial placodes and the hindbrain is achieved as the neuroglial hindbrain crest cells guide the epibranchial neuronal cells inward to establish their central connections. This work defines a role for the neuroglial hindbrain crest in organizing the afferent innervation of the hindbrain.

After regional specification, during which constituent parts of an embryonic field are defined, the next developmental challenge is that of integration, during which the different embryonic fields are coordinated, and thus, later anatomy and function established. Developmental integration is particularly apparent in the vertebrate head, because head development involves integration of a number of disparate embryonic cell types (1). Here, we studied in the chick the development of the epibranchial ganglia: the geniculate, petrosal, and nodose, which convey gustatory and viscerosensory information from the oro-pharyngeal cavity to central sensory nuclei in the hindbrain (Fig. 1, A and B) (2). The sensory neurons of these ganglia originate in the epibranchial placodes and connect to the central nervous system (CNS) (3, 4). These placodes are focal thickenings of ectoderm close to the tips of the pharyngeal pouches, and which are induced by the pharyngeal endoderm through the action of Bmp-7 (5). It has been unclear, however, how the neuronal cells generated by the epibranchial placodes migrate internally to the site of ganglion formation. We show here that this process is mediated by the neuroglial rhombencephalic neural crest. The epi-

branchial neuronal cells move inward along the tracks of neuroglial neural crest that extend from the hindbrain to the placodes. These results define a role for the neuroglial hindbrain neural crest in the integration of hindbrain and epibranchial placode development.

With a view toward understanding this process, we characterized the migratory paths taken by the epibranchial placodal cells as they move internally. The placodal cells were labeled by application of the lipophilic dye DiI to the exterior of the embryo, at stages concomitant with the induction of these placodes (6). This procedure results in the labeling of the embryonic ectoderm. Cells that leave this tissue layer carry the label with them as they move inward (Fig. 1). Cells migrating from both the geniculate and the petrosal placodes form organized streams extending from the placodal ectoderm toward the hindbrain (Fig. 1).

The migratory paths formed by the epibranchial neuronal cells are reminiscent of those formed by another group of cells, the neural crest. The neural crest cells in this region of the embryo migrate as segregated streams from specific axial levels of the hindbrain (Fig. 2A) (7, 8). The crest cells within these streams, however, have two distinct fates. The early ventrally migrating population fill the underlying pharyngeal arches and form ectomesenchymal derivatives within these structures, whereas the

Medical Research Council (MRC) Centre for Developmental Neurobiology, Fourth Floor, New Hunts House, Guys Campus, Kings College London, London SE1 9RT, UK.

*To whom correspondence should be addressed. E-mail: anthony.graham@kcl.ac.uk

REPORTS

later-migrating crest cells do not enter the arches and form neurons and glia (9). The neuroglial crest cells can be specifically visualized through their expression of a number of markers, such as the HMG transcription factor *Sox-10* (10). *Sox-10* labels the more dorsally located crest, which extends from the hindbrain toward the arches, whereas HNK-1 labels both these cells and the ectomesenchymal crest within the arches (Fig. 2) (8). The migratory epibranchial neuronal cells, which express *Phox-2a* (Fig. 2C) (11), overlap with the neuroglial neural crest. Double in situ hybridization with *Sox-10* to mark neuroglial crest cells and *Phox-2b* to mark epibranchial placodal cells (12) indicates that these two cell populations do follow the same path (Fig. 2, D and E). Tracking neural crest cells labeled with DiI and placodal cells labeled with DiO confirmed that epibranchial neuronal cells follow the neuroglial crest cells (Fig. 2F) (6).

These results suggest the possibility that the migratory epibranchial neuronal cells are guided by the neural crest. To test this hypothesis, we analyzed the effect of neural crest ablations on migration of epibranchial neuronal cells. We removed the hindbrain at stage 9 of development and then grew the embryos for either 24 or 48 hours (13). This manipulation results in the removal of the crest, as judged through lack of *Dlx-2*- and HNK-1-expressing cells [(Fig. 3, A and B) (14) ($n = 10$)]. In this situation, we found that the absence of crest perturbed the inward migration of the epibranchial neuronal cells. Even though *Phox-2a*-positive neural cells are evident, they do not move internally, but rather sit subectodermally (Fig. 3B; $n = 10$). Ablated embryos were also grown up for 48 hours after the operation to determine if the absence of the crest had any effects upon the differentiation of the epibranchial neuronal cells. We found that in these embryos, the epibranchial neuronal cells matured and sent out axons, but that these fibers made aberrant connections, often extending toward the adjacent ganglion (Fig. 3C; $n = 7$). We also analyzed the effect of removing one crest stream by ablating rhombomere 4, from which the second arch neural crest stream arises (7, 13). In these embryos, the development of the petrosal and nodose ganglia was largely unaffected, but the geniculate ganglion was perturbed. These neuronal cells remained subectodermal and again made aberrant connections, sending their axons to the otic vesicle (Fig. 3D; $n = 5$). In these small ablations, it was also apparent that the axons of the vestibuloacoustic ganglion did not establish their central projections (Fig. 3D). Because these ablations involved the removal of the hind-

brain along with the neural crest, it could be possible that this behavior is due to the lack of the CNS or its efferent motor axons,

rather than the neural crest cells. To test this hypothesis, we ablated segments of the neural tube at stage 12, after they had

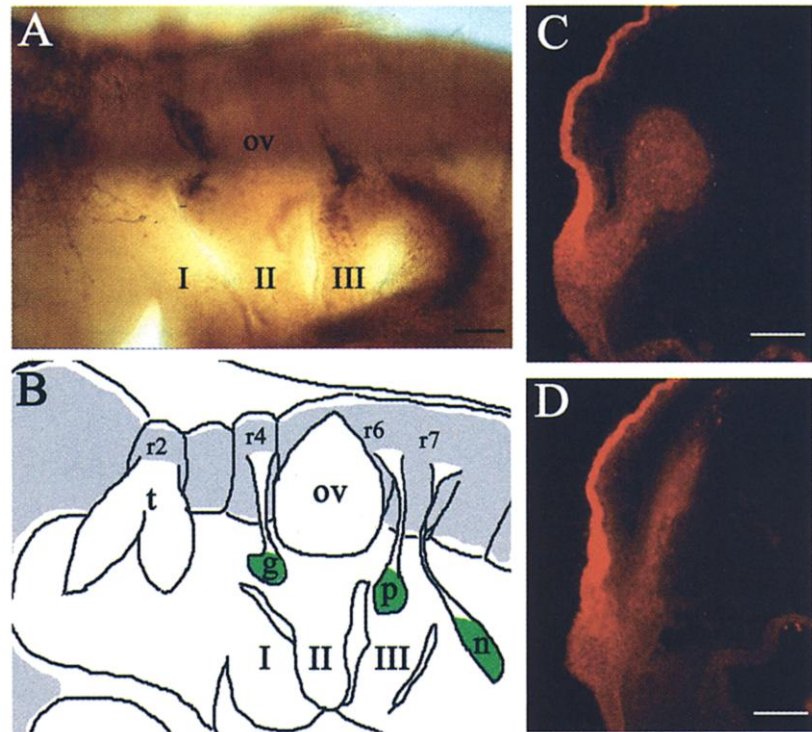


Fig. 1. Migration of the epibranchial neuronal cells. (A) Lateral view of a stage 17 chick embryo, immunostained for neurofilament medium chain (NF-M). NF-M-positive cells are seen within the epibranchial placodes, and migrating internally. Pharyngeal arches: I, II, and III; otic vesicle, ov. (B) Schematic representation of the epibranchial ganglia in relation to the pharyngeal arches, and the hindbrain. Geniculate ganglion, g; petrosal ganglion, p; nodose ganglion, n; trigeminal ganglion, t; rhombomeres: r2; r4; r6; and r7. (C and D) Dil-labeled placodal cells migrating away from DiI-labeled ectoderm in cross section at the level of the geniculate placode (C) and the petrosal placode (D). Bars in (A), (C), and (D): 140 μ m.

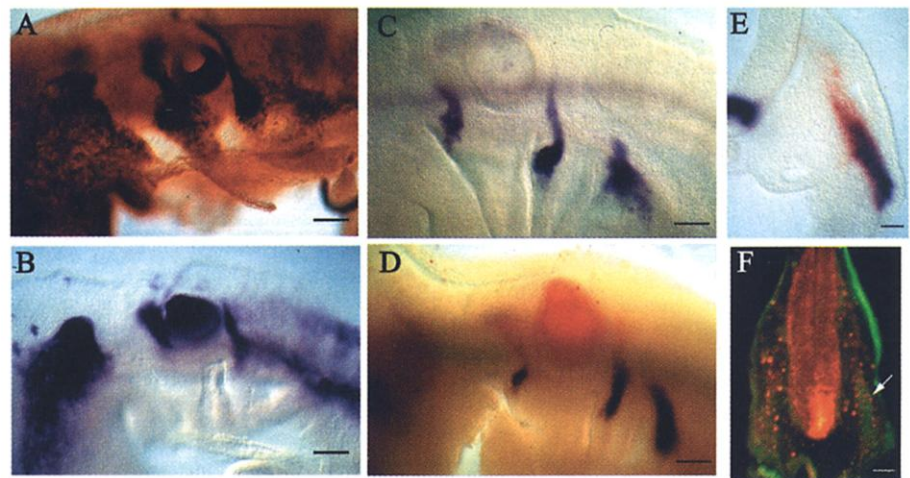


Fig. 2. Migration of the epibranchial neuronal cells overlaps with the neuroglial crest. [(A) to (D) are lateral views. (A) A stage 15 chick embryo, immunostained for HNK-1, which marks the majority of migrating neural crest in comparison to (B) *Sox-10* in situ hybridization, stage 16, which labels a subpopulation of neural crest cells. (C) *Phox-2a* in situ hybridization, stage 17, labels the epibranchial neuronal cells as they are born within the placodes, and migrate internally. (D) Double in situ hybridization, stage 17, *Sox-10* in red, and *Phox-2b* in blue. (E) Cross section through (D) at the level of the petrosal placode shows that the neuroglial crest (red), and the placodal neuronal cells (blue) overlap. (F) DiI labeling of the neural crest (red) and DiO labeling of the placodal cells (green) confirms that these two populations follow the same path (white arrows). Bars: (A) through (D), 140 μ m; (E), 45 μ m; (F), 90 μ m.

REPORTS

produced the neural crest (7, 15), but before their production of motor axons (16, 17). The consequence was that in the presence of the neural crest, but in the absence of the CNS tissue, the epibranchial neuronal cells moved internally and sent axons toward the CNS (Fig. 3, E and F; $n = 6$). However, because their central target was removed, these axons never connected and their fibers overshot and projected beyond the hindbrain (Fig. 3, E and F). Thus, the neural crest cells guide the epibranchial neuronal cells internally toward the CNS and enable their central connections.

Our results explain how integration between the epibranchial placodes and the hindbrain is established. The neuroglial neural crest cells thus are responsible for organizing the sensory innervation of the hindbrain, such that the geniculate ganglion, for example, forms between the second pharyngeal arch and the hindbrain, and that

its projections enter at the rhombomere 4 level. In our ablation experiments, the vestibuloacoustic and trigeminal ganglia also failed to connect to the hindbrain, suggesting that crest cells also control these connections.

A number of lines of evidence suggest that the segregation of the neural crest into separate streams is required for the patterning of the pharyngeal arches (18, 19). It has been proposed that each of these crest streams acquires distinct morphogenetic cues within the hindbrain, and that these are carried to the corresponding pharyngeal arches. However, it is now clear that pharyngeal arches can form, are regionalized, and have a sense of identity in the absence of neural crest (14, 20), and that arch patterning is more consensual than previously believed, with the crest acting in concert with endodermal and mesodermal cues (1, 20, 21). Furthermore, it has been shown that lampreys, which are jawless verte-

brates, exhibit streaming of hindbrain crest (22), which indicates that the streaming of the crest has a more ancestral role than separating the mandibular, first, arch crest from the hyoid, second, arch crest. Thus, it seems plausible that an ancestral role of crest streaming could be to organize the placodal innervation of the hindbrain, which could also have been later co-opted to help pattern the jaws and jaw-support of gnathostomes.

These results, coupled with our earlier studies, demonstrate how successive interactions can work to establish developmental integration. The sensory neurons of the epibranchial ganglia are believed to mediate gustatory and viscerosensory information for the oro-pharyngeal cavity to the solitary nucleus of the brain stem, and at each point in their formation there is a clear link between the developmental events and their later function. The epibranchial placodes are induced to form by the pharyngeal endoderm (5), which is believed to be subsequently innervated by the sensory neurons of the epibranchial ganglia, both generally and through the innervation of the taste buds, which arise autonomously from the pharyngeal endoderm (23). The neuronal cells that subsequently emerge from the placodes are directed inward, and their innervation of the hindbrain is guided by streams of neural crest cells arising from specific axial levels of the hindbrain. Thus, through developmental integration, the anatomical and functional relationships between the epibranchial ganglia and their central and peripheral targets are established.

References and Notes

1. A. Graham, A. Smith, *Bioessays* **23**, 54 (2001).
2. C. U. Ariens Kappers, G. C. Huber, E. C. Crosby, *The Comparative Anatomy of the Nervous System of Vertebrates, Including Man* (Hafner, New York, 1960).
3. C. S. Ayer-Le Lievre, N. M. Le Douarin, *Dev. Biol.* **94**, 291 (1982).
4. A. D'Amico-Martel, D. M. Noden, *Am. J. Anat.* **166**, 445 (1983).
5. J. Begbie, J. F. Brunet, J. L. Rubenstein, A. Graham, *Development* **126**, 895 (1999).
6. For labeling of placodal cells, Dil (1,1'-dilinoleyl-3,3,3',3'-tetramethylindocarbocyanine perchlorate, 10 mg/ml in ethanol) was diluted 1:10 in 0.3 M sucrose, and 3 μ l was applied in ovo to embryos at stage 16. The embryos were reincubated for 24 to 48 hours, and were subsequently fixed, embedded in 7.5% gelatin and 15% sucrose, and cryosectioned at 10 μ m. For double labeling, the Dil was injected into the lumen of the neural tube of embryos at stage 9, and the embryos were incubated for 24 hours, then 3 μ l of DiO (as described for the Dil) was applied in ovo. Embryos were treated as for single Dil labeling.
7. A. Lumsden, N. Sprawson, A. Graham, *Development* **113**, 1281 (1991).
8. Whole-mount immunostaining and whole-mount in situ hybridization, both single and double, were carried out as described (5).
9. C. V. Baker, M. Bronner-Fraser, N. M. Le Douarin, M. A. Teillet, *Development* **124**, 3077 (1997).
10. S. Britsch *et al.*, *Genes Dev.* **15**, 66 (2001).
11. X. Morin *et al.*, *Neuron* **18**, 411 (1997).
12. A. Pattyn, X. Morin, H. Cremer, C. Goridis, J. F. Brunet, *Nature* **399**, 366 (1999).
13. Neural crest ablations were carried out as described (5), but embryos were reincubated for either 24 or 48 hours.

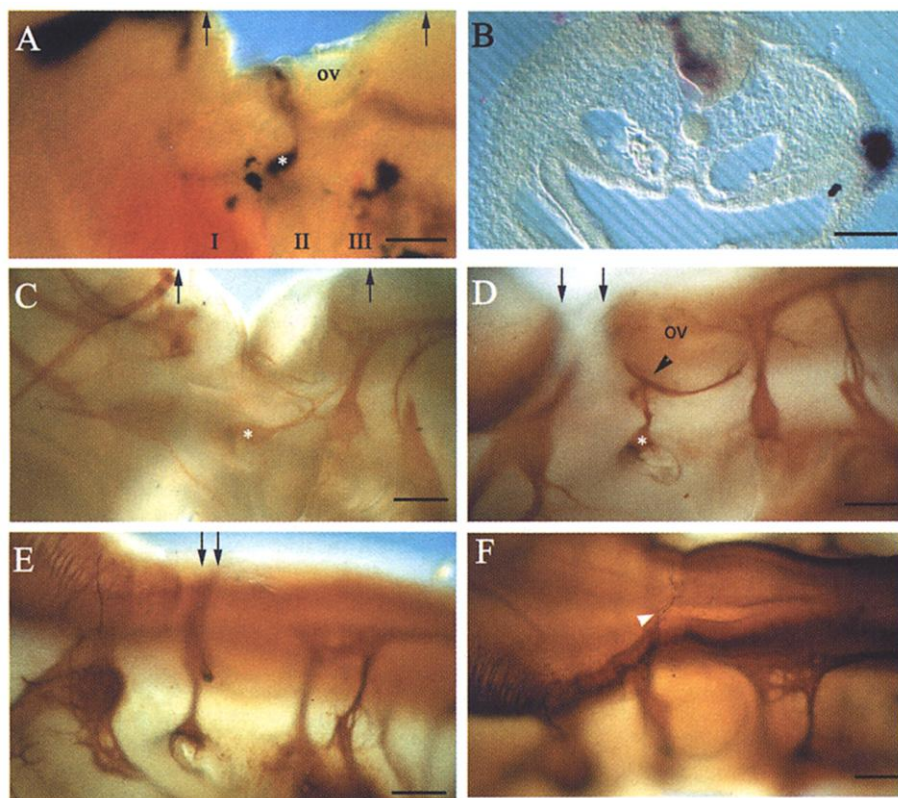


Fig. 3. Migration of the placodal neuronal cells is dependent on the neural crest. (A) Lateral view of an embryo 24 hours after neural tube ablation; arrows mark the extent of the ablation. Double in situ hybridization using *Dlx-2* to mark neural crest (red) and *Phox-2a* (blue) to mark placodal cells shows that the epibranchial placodes form normally in the absence of crest (*). Pharyngeal arches: I, II, and III; otic vesicle, ov. (B) Section through (A) at the level of the geniculate placode shows that the placodal cells fail to migrate internally. (C) Lateral view of an embryo 48 hours after ablation. NF-M staining shows that the geniculate ganglion forms (*), but is superficial and fails to connect to the hindbrain. (D) Lateral view of an embryo 24 hours after r4 ablation, but before crest migration. The geniculate ganglion is superficial (*) and fails to connect to the hindbrain. The black arrowhead marks the position of the forming vestibuloacoustic ganglion. (E) Lateral view of embryo 24 hours after r4 ablation, and after crest migration. The geniculate ganglion forms normally, and sends projections toward the hindbrain. (F) Dorsal view of (E) shows that although these axons pathfind correctly toward their target, they overshoot and pass over the hindbrain (white arrowhead). Bars: (A), (B), (E), and (F), 140 μ m; (C) and (D), 280 μ m.

To ablate the second arch crest stream, we removed rhombomere 4 and portions of the adjacent rhombomeres 3 and 5 at stage 9/10. Later hindbrain ablations were performed at stage 12, the whole neural tube was removed at the level of rhombomere 4 using a fire-sharpened tungsten needle, and the embryos were reincubated for 24 hours.

14. E. Veitch, J. Begbie, T. F. Schilling, M. M. Smith, A. Graham, *Curr. Biol.* **9**, 1481 (1999).
15. K. W. Tosney, *Dev. Biol.* **89**, 13 (1982).
16. A. Lumsden, R. Keynes, *Nature* **337**, 424 (1989).
17. H. Simon, S. Guthrie, A. Lumsden, *J. Neurobiol.* **25**, 1129 (1994).
18. D. M. Noden, *Dev. Biol.* **96**, 144 (1983).
19. A. Graham, I. Heyman, A. Lumsden, *Development* **119**, 233 (1993).
20. T. Piotrowski, C. Nusslein-Volhard, *Dev. Biol.* **225**, 339 (2000).
21. P. Trainor, R. Krumlauf, *Nature Cell Biol.* **2**, 96 (2000).
22. N. Horigome *et al.*, *Dev. Biol.* **207**, 287 (1999).
23. L. A. Barlow, R. G. Northcutt, *Development* **124**, 949 (1997).
24. We thank P. Scotting for the *Sox-10* probe and A. Lumsden for critical comments on this manuscript. This work was funded by the UK MRC.

27 April 2001; accepted 2 August 2001

Crystal Structure of an Early Protein-RNA Assembly Complex of the Signal Recognition Particle

Klemens Wild,^{1*} Irmgard Sinning,¹ Stephen Cusack²

The signal recognition particle (SRP) is a universally conserved ribonucleoprotein complex that mediates the cotranslational targeting of secretory and membrane proteins to cellular membranes. A crucial early step in SRP assembly in archaea and eukarya is the binding of protein SRP19 to specific sites on SRP RNA. Here we report the 1.8 angstrom resolution crystal structure of human SRP19 in complex with its primary binding site on helix 6 of SRP RNA, which consists of a stem-loop structure closed by an unusual GGAG tetraloop. Protein-RNA interactions are mediated by the specific recognition of a widened major groove and the tetraloop without any direct protein-base contacts and include a complex network of highly ordered water molecules. A model of the assembly of the SRP core comprising SRP19, SRP54, and SRP RNA based on crystallographic and biochemical data is proposed.

Proteins that are inserted in or transported through membranes contain an NH₂-terminal signal sequence, which is cotranslationally recognized by the universally conserved signal recognition particle (SRP) (1). SRP is a cytoplasmic ribonucleoprotein particle (RNP) that binds the signal sequence as it emerges from the ribosome and targets the nascent chain-ribosome complex to the endoplasmic reticulum (ER) in eukaryotes or to the plasma membrane in prokaryotes (2).

In higher eukaryotes, SRP contains six proteins and can be split into two domains—the *Alu* domain and the *S* domain—that are linked by the SRP RNA consisting of ~300 nucleotides (nt) (Fig. 1A) (1). Whereas the *Alu* domain is responsible for retarding the ribosomal elongation of the nascent chain during targeting, the *S* domain forms the functional core by binding to the signal sequence and mediating the docking to the translocation machinery in the ER membrane in a guanosine 5'-triphosphate (GTP)-dependent process (1). The *S* domain consists of the

four larger proteins SRP19, the GTPase SRP54, and the SRP68/72 heterodimer, as well as the central part of the SRP RNA.

SRP19 is an essential player in the assembly of SRP (3) and binds to free SRP RNA already in the nucleolus (4). This early assembly event is a prerequisite for the binding of SRP54 to helix 8 of SRP RNA in eukaryotes (3) and involves an SRP19-induced conformational change in the RNA (5). Genome-based sequence alignments indicate that SRP19 homologs are present only in organisms whose SRP RNA contains helix 6 (6), which has been identified as the primary binding site of SRP19 (7). Helix 6 is closed by a tetranucleotide hairpin loop (tetraloop) of the unusual GNAR (N: any nucleotide, R: either G or A) sequence fingerprint (7). The adenine at the third position is strictly conserved and has been shown to be essential for SRP19 binding (7). Little structural information is available about how SRP19 binds to and reorganizes the SRP RNA to form an SRP core particle. Here we present the 1.8 Å resolution crystal structure of the human SRP19 in complex with a distal fragment of helix 6 that includes the GGAG tetraloop. Together with chemical footprint data (8, 9), the structure allows us to propose a model for the assembly of the SRP core.

To obtain crystals of the protein-RNA complex, we removed the 24 COOH-terminal residues of SRP19 that were shown to be dispens-

able for RNA binding (10) and are not conserved in the archaeal protein (6). The RNA corresponds to the same 29-nt fragment of helix 6 previously used for structure determination of the uncomplexed RNA (11), and initial, but poor, phases could therefore be obtained by the molecular replacement method. The structure was finally solved by a single-wavelength anomalous dispersion (SAD) experiment with 5-bromouridine-labeled RNA (11). Procedures are described in (12) and data and model statistics are listed in Table 1.

The structure reveals a complex protein-RNA interface in which long, presumably flexible, loops of SRP19 recognize the particular shape of the rather rigid stem-loop RNA (Fig. 1B). SRP19 is a single-domain αβ-type protein with a central three-stranded antiparallel β sheet packed on one side against two helices. It has a βαββα topology with the COOH-terminal β strand in the middle of the β sheet, similar to the K-homology (KH) domain (13), but quite different from the αβββα topology found, for example, in the double-stranded RNA binding domain (13) or in SRP9 and SRP14 (14). SRP19 sits on the tip of helix 6 with the β1 edge of the β sheet contacting the GGAG tetraloop. Two extended loop regions (L1 and L3) with short interspersed 3₁₀ helices and several conserved sequence motifs [(sequence comparisons are shown in Web fig. 1 (15)] fill the adjacent and extremely wide major groove of the RNA, which originates from a tandem A·C/C·A mismatch and a G·U wobble base pair all opening toward the major groove (Fig. 1B). Protein-RNA interactions without any direct base recognition and a complex network of highly ordered water molecules characterize the molecular interface. Previous results on the effect of mutagenesis on SRP19 binding to SRP RNA, either systematic (16) or of conserved basic residues (17), are consistent with the structure. The tight binding of SRP19 to the RNA leaves, however, the last three bases of the tetraloop, 148-GAG, solvent-exposed with the potential to form RNA-RNA tertiary interactions.

The unusual GNAR-type tetraloop is the most highly conserved region of SRP RNA helix 6 [see supplementary material (15)]. Hairpins containing tetraloops are extremely common to large RNA molecules (18) and are thought to function as nucleation sites to ensure proper RNA folding and especially RNA-RNA tertiary interactions (19). The GNRA tetraloops are most common (18) and the first atomic-

¹Biochemie-Zentrum (BZH), University of Heidelberg, Im Neuenheimer Feld 328, D-69120 Heidelberg, Germany. ²European Molecular Biology Laboratory Grenoble Outstation, BP 181, F-38042 Grenoble Cedex 9, France.

*To whom correspondence should be addressed. E-mail: klemens.wild@bzh.uni-heidelberg.de